ResearchGate

See discussions, stats, and author profiles for this publication at: https://www.researchgate.net/publication/256499600

Hollow Structured Li3VO4 Wrapped with Graphene Nanosheets in Situ Prepared by a One-Pot Template-Free Method as an Anode for Lithium-Ion Batteries

ARTICLE *in* NANO LETTERS · SEPTEMBER 2013

Impact Factor: 13.59 · DOI: 10.1021/nl402237u · Source: PubMed

CITATIONS
76

READS
71

8 AUTHORS, INCLUDING:

Shu-Lei Chou
University of Wollongong
123 PUBLICATIONS **3,200** CITATIONS
SEE PROFILE

David Wexler
University of Wollongong
174 PUBLICATIONS **4,935** CITATIONS
SEE PROFILE

Hua-Kun Liu
University of Wollongong
269 PUBLICATIONS **9,053** CITATIONS
SEE PROFILE

Yuping Wu
Fudan University
240 PUBLICATIONS **8,047** CITATIONS
SEE PROFILE

Available from: Yuping Wu
Retrieved on: 03 February 2016

NANO LETTERS

Letter

pubs.acs.org/NanoLett

Hollow Structured Li_3VO_4 Wrapped with Graphene Nanosheets in Situ Prepared by a One-Pot Template-Free Method as an Anode for Lithium-Ion Batteries

Yi Shi,[†,‡] Jia-Zhao Wang,*[,‡] Shu-Lei Chou,[‡] David Wexler,[§] Hui-Jun Li,[∥] Kiyoshi Ozawa,[⊥] Hua-Kun Liu,[‡] and Yu-Ping Wu*[,†]

[†]New Energy and Materials Laboratory (NEML), Department of Chemistry & Shanghai Key Laboratory of Molecular Catalysis and Innovative Materials, Fudan University, Shanghai 200433, China

[‡]Institute for Superconducting and Electronic Materials, University of Wollongong, Wollongong, New South Wales 2522, Australia

[§]Electron Microscopy Centre, Innovation Campus, University of Wollongong, Wollongong, New South Wales 2522, Australia

[∥]Faculty of Engineering, University of Wollongong, Wollongong, New South Wales 2522, Australia

[⊥]National Institute for Materials Science, Tsukuba, Ibaraki Prefecture 305-0047, Japan

Supporting Information

ABSTRACT: To explore good anode materials of high safety, high reversible capacity, good cycling, and excellent rate capability, a Li_3VO_4 microbox with wall thickness of 40 nm was prepared by a one-pot and template-free in situ hydrothermal method. In addition, its composite with graphene nanosheets of about six layers of graphene was achieved. Both of them, especially the Li_3VO_4/graphene nanosheets composite, show superior electrochemical performance to the formerly reported vanadium-based anode materials. The composite shows a reversible capacity of 223 mAh g^{-1} even at 20C (1C = 400 mAh g^{-1}). After 500 cycles at 10C there is no evident capacity fading.

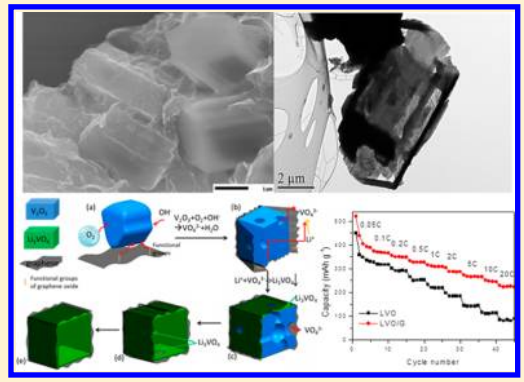

KEYWORDS: *Lithium vanadium oxide, graphene, nanosheet, hollow structure, anode, lithium ion battery*

Developing a sustainable and renewable energy future has been one of the most important tasks for worldwide scientists to address increasing global energy consumption as well as the critical issue of climate change. Efficient energy storage systems are needed for the electricity generated from intermittent, renewable sources.[1] Rechargeable lithium ion batteries have been commercially successful energy storage devices since 1991.[2] So far, there are three main anode materials: the alloy-type anodes materials such as Si- and Sn-based alloys and their composites,[3] the conversion reaction type ones such as transition metal oxides,[4,5] and the intercalation/deintercalation type one such as graphite, Ti-based oxides,[6] and layered V-based oxides.[6,7] Although work on the alternatives to intercalation type anode materials has made important progress, graphite still remains the dominant commercial anode material. However, graphite has a small lithium diffusion coefficient and experiences a large volume variation of 9% during the lithium intercalation/deintercalation process. In addition, it has severe safety issues of dendritic lithium growth, due to its low potential (only about 0.2 V versus Li^+/Li). Especially at high rates, polarization would considerably lower its potential further, causing the birth of lithium dendrites and the consequent safety issues. Furthermore, the thick solid electrolyte interphase (SEI) layer on its surface could also introduce kinetic problems for fast charge and discharge.[8] $Li_4Ti_5O_{12}$ has been found to change its structure negligibly during the discharge/charge process and possesses good lithium ion mobility and a long and stable voltage plateau, together with low cost, environmental friendliness, and enhanced safety.[8−10] Nevertheless, its potential is still relatively higher, about 1.6 V (versus Li^+/Li), thus halving the overall cell voltage and negating the benefits. The estimated energy density of lithium ion batteries based on the $Li_4Ti_5O_{12}$ anode (regarding both potential and capacity) does not exceed one-third of that on graphite if they are coupled with a typical 4 V cathode.[5] It was recently reported that Li can be intercalated into the layered transition metal oxide $LiVO_2$,[6] but its major difficulty for application as an anode lies in the fast deterioration of the material.[11−13] So, it would be of great interest to find a new intercalation anode with large capacity and appropriate intercalation potential.[5]

Received: June 19, 2013
Revised: September 1, 2013
Published: September 11, 2013

ACS Publications © 2013 American Chemical Society

Scheme 1. Schematic Illustration Summarizing All of the Major Morphological Changes Involved in the Synthesis of LVO/G by Corrosive Etching[a]

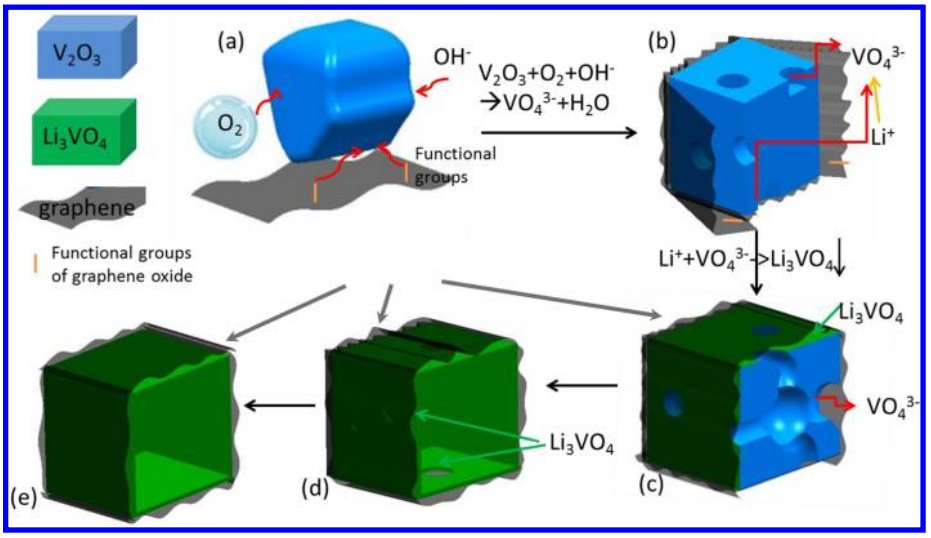

[a]:(a) Commercial V_2O_3 microrod; (b) pitting at several specific sites on the surface of such a microrod, where the O_2 dissolved in the solvent and the functional groups of graphene oxide have oxidized the V_2O_3; (c) cross-section of hollow structure after further etching of the interior of the rod and its covering with Li_3VO_4 precipitate; (d) subsequent hollowing of the rod; (e) formation of a completely enclosed Li_3VO_4 microbox wrapped with graphene nanosheets.

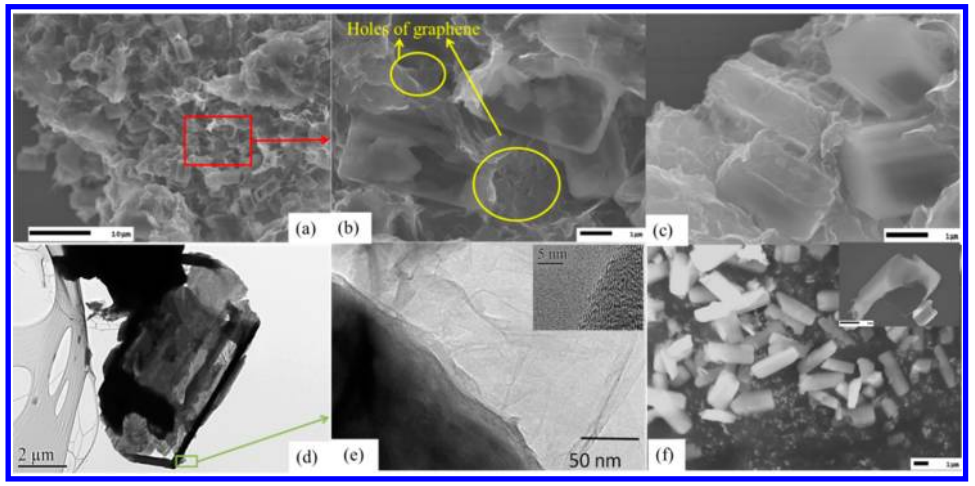

Figure 1. Electronic micrographs of LVO/G composite measured by a field emission scanning electron microscopy (FE-SEM: JEOL JSM-7500FA; TEM: JEOL 2011 high-resolution instrument): (a) FESEM secondary electron micrograph of large area of LVO/G; (b) FESEM micrograph of the area indicated by the rectangle marked with red lines in Figure 1a; (c) FESEM micrograph of LVO/G; (d) TEM micrograph of hollow LVO/G; (e) graphene region attached to Li_3VO_4 (lower right) with the inset of HRTEM micrograph of edge of graphene, revealing contrast from C-type fringes, and (f) FESEM micrograph of LVO with the inset showing a broken Li_3VO_4 microbox.

Recently, it was reported that $Li_3VO_4^+$ intercalates Li ions mainly in the voltage range between 0.5 and 1.0 V vs Li/Li^+, lower than the potential of $Li_4Ti_5O_{12}$ and higher than that of graphite. Its theoretical capacity is 394 mAh g^{-1}, in accordance with $x = 2$ in $Li_{3+x}VO_4$. Combined with the low and safe voltage, Li_3VO_4 features a large specific capacity and low cost. It might act as a new intercalation anode for the lithium ion battery.[5] Despite these advantages, the practical use of this material still faces some barriers. Li_3VO_4 requires further modifications to overcome certain limitations, such as low electronic conductivity, which is quite lower compared to its ionic conductivity, and this may cause large resistance polarization and poor rate capability. Thus, reducing the particle size and hybridization with electronically conductive materials are necessary for this material to be suitable for future use.[5]

The properties of inorganic hollow structures can be well-tuned by tailoring their morphology and crystallinity.[14−16] However, it is a great challenge to develop feasible methods for the one-pot, template-free, solution synthesis of single-crystalline particles with well-defined nonspherical morphologies.[17] Here, we reported the preparation of a composite of hollow Li_3VO_4 microboxes with a wall thickness of about 40 nm wrapped by graphene nanosheets (LVO/G). When the LVO/G composite is used as anode material for lithium ion batteries, it offers significant improvements in capacity, rate capability, and cycling life compared to the reported vanadium-based anode materials.[5,13]

dx.doi.org/10.1021/nl402237u | *Nano Lett.* 2013, 13, 4715−4720

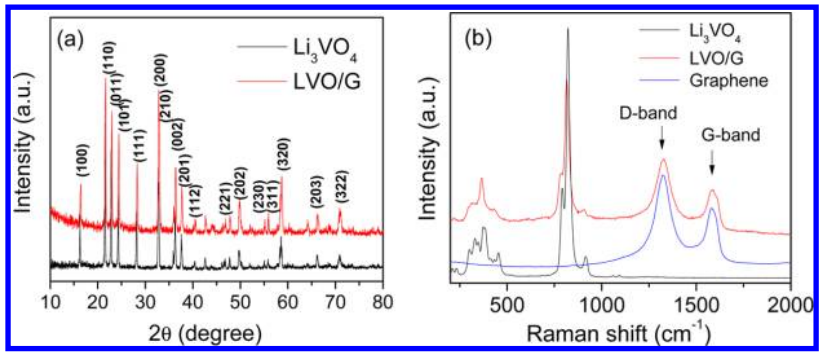

Figure 2. (a) XRD patterns of the prepared Li_3VO_4 microboxes and the LVO/G composite which were measured by using a GBC MMA instrument with Cu Kα radiation and a graphite monochromator. Data were collected from powder samples at a scanning rate of 3 deg min^{-1} for 2θ in the range of 10−80°; and (b) Raman spectra of the graphene, the Li_3VO_4 microboxes, and the LVO/G composite obtained by using a Jobin Yvon HR800.

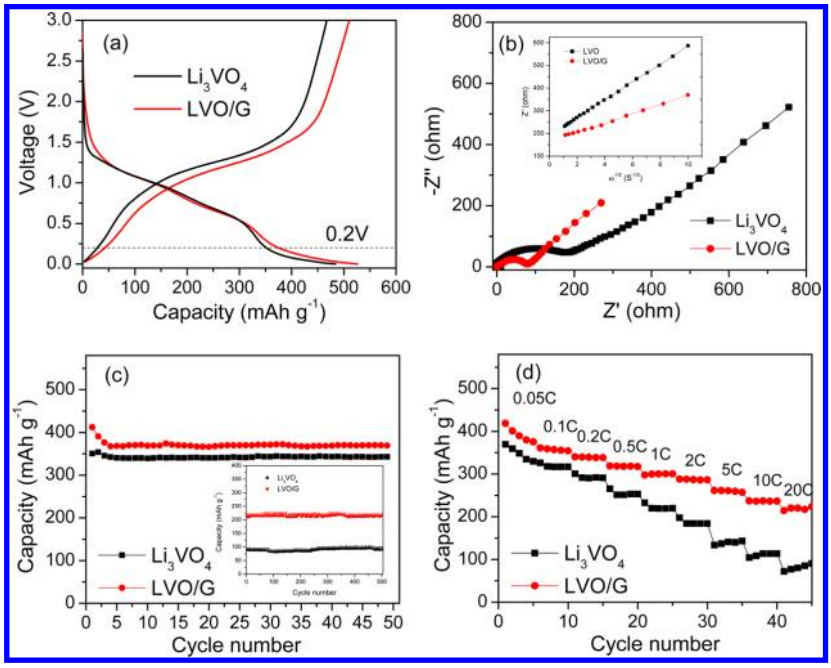

Figure 3. Electrochemical performance of the Li_3VO_4 and the LVO/G composite tested by using the electrodes prepared by pasting the mixture of the Li_3VO_4 or LVO/G anode material, carbon black, and sodium carboxymethyl cellulose (CMC) in a weight ratio of 75:20:5 on a copper foil followed by a drying in a vacuum oven at 150 °C for 2 h. CR 2032 coin-type cells were assembled in an Ar-filled glovebox (Mbraun, Unilab, Germany) using lithium metal foil as the counter and reference electrode and 1 M $LiPF_6$ solution in ethylene carbonate/diethyl carbonate as the electrolyte: (a) typical discharge and charge profiles at the current density of 20 mA g^{-1} between the voltage range of 0 and 3 V measured by a Land Battery Tester; (b) Nyquist plots of the anodes after five cycles with the real parts of the complex impedance versus $\omega^{-1/2}$ at an anodic potential of 0.75 V (vs Li^+/Li) (inset) (Biologic VMP3 electrochemical workstation, the AC amplitude was 5 mV, and the frequency range applied was 0.01 Hz to 100 kHz); (c) cycling performance at the current density of 20 mA g^{-1} between the voltage range of 0.2 and 3 V, and the inset is their cycling performance at 10C (4 A g^{-1}); and (d) rate performance between the voltage range of 0.2 and 3 V.

At first, graphene oxide (GO) was prepared according to the method reported by Hummers from graphite powder (Aldrich, powder, < 20 μm, synthetic).[17] Then the LVO/G composite was prepared by an in situ one-step hydrothermal process as shown in Scheme 1. In a typical synthesis, a suitable amount of GO, hydrazine hydrate, 1.688 g of LiOH, 0.304 g of V_2O_3 (>99.0%, Sigma−Aldrich), and deionized H_2O were mixed together for 2 h using an ultrasonic probe, which was followed by vigorous magnetic stirring at room temperature for 0.5 h. The resultant mixture was then transferred to an autoclave and kept in an oven at 180 °C for 40 h under a vacuum pressure of 0.1 MPa. The product was washed with deionized water, anhydrous ethanol, and acetone several times and dried at 80 °C in a vacuum oven for 4 h. For comparison, Li_3VO_4 microboxes was also prepared using the same procedure without graphene oxide and hydrazine hydrate, and graphene was obtained by the reduction of graphene oxide with hydrazine hydrate. As to the detailed formation mechanism of the microboxes (Scheme 1), the Supporting Information (Figures S1 and S2) can be referred. The main action is due to the hollowing of the initial microrods by an oxygen-engaged oxidation process from V_2O_3 into VO_4^{3-},[14] and the precipitating of the soluble VO_4^{3-} anions on the surface of the V_2O_3 cubes as Li_3VO_4.[18]

Electronic micrographs (Figure 1) of the LVO/G composite indicates that the sample comprises of Li_3VO_4 microboxes and graphene nanosheets. The average size of the Li_3VO_4 microboxes is around 2 μm in length, 800 nm in width, and 500 nm in height. Its wall thickness is around 40 nm (Figure 1f). The hollow structure of the Li_3VO_4 microboxes and holes

dx.doi.org/10.1021/nl402237u | Nano Lett. 2013, 13, 4715−4720

between the graphene nanosheets can easily be filled with electrolyte, which is expected to offer rapid routes for both Li^+ ion and electron transportation. The surface of the hollow LVO microboxes is wrapped with graphene nanosheets of about six layers in thickness (Figure 1d and e). It should be emphasized that, even after a long period of sonication during the preparation of the FESEM and TEM specimens, the graphene nanosheets are still anchored on the surface of the Li_3VO_4 microboxes, suggesting that their interaction is strong.[19]

X-ray diffraction (XRD) patterns for the Li_3VO_4 microboxes and the LVO/G composite (Figure 2a) show that most diffraction lines can be indexed to the orthorhombic Li_3VO_4 phase (JCPDS No. 38-1247) with the lattice parameters a = 5.447 Å, b = 6.327 Å, c = 4.948 Å, and $\alpha = \beta = \gamma = 90°$. Diffraction peaks which might appear for graphene are absent, most likely because they are below the limits of detection by XRD, or the graphene (002) peak is eclipsed by the Li_3VO_4 (111) one. Another reason is that the layers of graphene sheets is too few, about 6 as the above-mentioned, and their diffraction intensity is very weak. Raman spectra (Figure 2b) indicate the existence of Li_3VO_4 and graphene in the composite. The bands in the range of 1200−1460 cm^{-1} and 1470−1730 cm^{-1} are attributed to the D-band (K-point phonons of A_{1g} symmetry) and G-band (E_{2g} phonons of C sp^2 atoms) of graphene. The broadening of the D and G bands with a strong D line indicates localized in-plane sp^2 domains and disordered graphitic crystal stacking of the graphene nanosheets. The peak intensity ratio between the 1333 and 1592 cm^{-1} peaks (I_D/I_G) generally provides a useful index about the degree of crystallinity of various carbon materials, that is, the smaller the I_D/I_G ratio, the higher the degree of ordering in the carbon material.[20] The I_D/I_G values of the graphene and the LVO/G composite are 1.633 and 1.638, respectively, indicating that the graphene nanosheets are well-retained even after their wrapping on the Li_3VO_4 microboxes.[21,33] The amount of graphene in the LVO/G composite was estimated to be approximately 10.5 wt % from the thermogravimetric analysis (Figure S3).

The electrochemical performance of the Li_3VO_4 microboxes and the LVO/G composite is shown in Figure 3. The gentle slope in the charge/discharge curves of the LVO/G composite may be attributed to the graphene. Both of them show a great overlapping above 0.2 V in the charge/discharge curves (Figure 3a). The charge (reversible) capacity of the LVO/G composite is 511 mAh g^{-1} (based on the weight of the composite) between 0 and 3.0 V, 44 mAh g^{-1} higher than that of the Li_3VO_4 microboxes, and the main capacity is situated between 0.2 and 2.0 V. These data are much higher than those of the reported.[5,13] The main capacity is situated at about 1 V, which is consistent with their cyclic voltammograms (Figure S4). In addition, the Li_3VO_4 also shows a discharge platform below 0.2 V, which makes the whole discharge capacity reach 467 mAh g^{-1}, much higher than that of the commercial graphite. The comparison of the discharge/charge profiles between different voltage range is shown in Figure S5. Considering that the amount of graphene is 10.5 wt %, the above comparison indicates that the contribution of graphene to capacity is not small, which will be about 440 mAh g^{-1} for the graphene nanosheets. This is similar to that for the reported amorphous carbon, whose voltage ranges from 0 to 3.0 V.[24] As a result, the intercalation and deintercalation reactions during the charge and discharge process can be shown as eq 1:

$$Li_3VO_4 + xLi^+ + xe^- \rightleftharpoons Li_{3+x}VO_4 \qquad (0 \le x \le 2) \tag{1}$$

The Nyquist plots (EIS spectra) show two compressed semicircles in the high to medium frequency range of each spectrum, which describe the charge transfer resistance (R_{ct}) for these electrodes, and an approximately 45° inclined line in the low-frequency range, which could be considered as Warburg impedance (Z_W), which is associated with the lithium-ion diffusion in the bulk of the active material. The first compressed semicircle is related to the SEI film, and the high-frequency intercept of the second semicircle is related to the uncompensated resistance (R_u), while the diameter of the second semicircle is related to the charge transfer resistance (R_{ct}).[22] After simulating the second compressed semicircle for both samples, the values of R_{ct} for the Li_3VO_4 and LVO/G electrodes after five cycles were calculated to be 211 and 80 Ω, respectively. The lithium diffusion coefficient can also be calculated by using the following equation:

$$D = R^2T^2/2A^2n^4F^4C^2\sigma^2 \tag{2}$$

where R is the gas constant, T is the absolute temperature, A is the surface area of the anode (1 cm^2), n is the number of electrons transferred in the half-reaction for the redox couple, F is the Faraday constant, C is the concentration of Li ions in the solid (9.8×10^{-3} mol cm^{-3}), D is the diffusion coefficient (cm^2 s^{-1}), and σ is the Warburg factor, which is relative to Z_{re}. From the slope of the lines in the inset of Figure 3b σ can be obtained.[23]

$$Z_{re} = R_D + R_L + \sigma\omega^{-1/2} \tag{3}$$

According to the linear fitting, the slope of the real part of the complex impedance versus $\omega^{-1/2}$ at the potential of 0.75 V (vs Li/Li^+) for the Li_3VO_4 and LVO/G electrodes after five cycles is 39.3 and 20.1, respectively. The lithium diffusion coefficients at 25 °C were calculated to be 2.37×10^{-13} and 9.18×10^{-13} cm^2 s^{-1} for the Li_3VO_4 and the LVO/G composite, respectively. These results show that the LVO/G composite presents smaller charge transfer resistance and higher lithium diffusion coefficient, which are favorable for rapid charge and discharge.

After the first few cycles, the electrode reactions show high reversibility (Figure 3c). The charge capacity of the third cycle of the Li_3VO_4 between the voltage range of 0.2 and 3 V is 345 mAh g^{-1}, and it remains very stable after 50 cycles. The cycling performance is superior to that of another newly reported vanadium-based insertion anode material, $LiVO_2$, whose capacity dropped from 350 to 100 mAh g^{-1} after 10 cycles,[6,11,12] and that of the reported Li_3VO_4,[5,13] whose capacity faded from the crack of crystal. In the case of the Li_3VO_4/graphene composite, it shows an even higher capacity. The charge capacity of the LVO/G composite in the third cycle is 378 mAh g^{-1} and does not fade evidently after 50 cycles, which is very near to its theoretical capacity, 394 mAh g^{-1}. After long cycling at high rate (10C), the capacity is still stable. The good retention of capacity can also be proved by the stable EIS spectra and tact SEM micrographs after cycling (Figure S6).

To compare the rate capability, the C rate is based only on the Li_3VO_4 and 1C is 400 mA g^{-1}. The Li_3VO_4 can retain a reversible capacity of 87 mAh g^{-1} at 20C. In contrast, the LVO/G composite exhibits an obviously much improved performance over the Li_3VO_4 (Figure 3d). A high charge capacity of 223 mAh g^{-1} was obtained for the LVO/G composite at the

dx.doi.org/10.1021/nl402237u | Nano Lett. 2013, 13, 4715−4720

current density of 20C, which is 136 mAh g^{-1} higher than that of the LVO. These results are also superior to the reported vanadium-based anode materials[5,13] and superior to those of graphite.

The improvement in the electrochemical performance of the Li_3VO_4 over the reported vanadium-based anode materials can be due to several factors. First, the cavities or holes in the hollow structure may provide extra space for the storage of lithium ions like in carbons,[24] which is beneficial for enhancing the specific capacity, and this is the main reason the reversible capacities of the Li_3VO_4 microboxes and the LVO/G composite are higher than the theoretic value of Li_3VO_4. Second, the hollow structure is often associated with larger surface area, which provides more sites for lithium insertion−desertion, leading to good charge and discharge performance at large current densities.[25] Third, the nanometer (40 nm) wall effectively reduces the diffusion distance for lithium ions, leading to better rate capabilities. Fourth, the void space in the hollow structures buffers the local volume change during lithium insertion−desertion and is able to alleviate the problem of pulverization and aggregation of the electrode material, hence keeping structural stability during cycling.[25,26]

In the case of the LVO/G composite, its superior electrochemical performance is ascribed to the wrapped graphene nanosheets. First, it provides higher electronic conductivity leading to the reduced charge transference resistance.[21,22] Second,[27,28] the high chemical diffusivity of Li on a graphene plane favors the transportation of lithium ions.[21,29−35] Third, the grapene nanosheets have the open and flexible porous structure favoring the emission the strain/stress and the retaining good structural stability during cycling.[32,35]

In summary, a composite of Li_3VO_4/graphene has been synthesized by a novel rapid one-step in situ hydrothermal method. The resultant composite reveals a unique morphology, in which homogeneous hollow structured Li_3VO_4 microboxes of 40 nm wall thickness are wrapped with porous graphene nanosheets. The hollow structure could relax the stress/strain of Li^+ insertion/deinsertion, increase the surface area of the materials, provide extra space for the storage of lithium ions, and reduce the effective diffusion distance for lithium ions. As a result, improved capacity, rate capability, and cycling performance have been achieved for the Li_3VO_4 microboxes. Furthermore, this graphene-wrapped nanoarchitecture provides high electronic conductivity for both facile mass transfer and facile charge transfer and good structural stability for the Li_3VO_4 microboxes. The Li_3VO_4/graphene composite has superior electrochemical performance such as high capacity, stable cycling life, and exceptional good rate capability. Therefore, the Li_3VO_4/graphene nanosheets composite is a promising anode candidate for the development of high-performance, low-cost, and advanced lithium batteries.

■ ASSOCIATED CONTENT

Supporting Information

Materials, methods, and addition supplemented figures. This material is available free of charge via the Internet at http://pubs.acs.org.

■ AUTHOR INFORMATION

Corresponding Author

*E-mail: wuyp@fudan.edu.cn.

Notes

The authors declare no competing financial interest.

■ ACKNOWLEDGMENTS

Financial support from an Australian Research Council (ARC) Discovery Project (DP100103909) and the National Natural Science Foundation of China (NSFC) (21073046) is greatly appreciated. Many thanks also go to Dr. Tania Silver for critical reading of the manuscript.

■ REFERENCES

(1) Yu, G.; Hu, L.; Vosgueritchian, M.; Wang, H.; Xie, X.; McDonough, J. R.; Cui, X.; Cui, Y.; Bao, Z. *Nano Lett.* **2011**, *11* (7), 2905−2911.
(2) Cui, L.-F.; Ruffo, R.; Chan, C. K.; Peng, H.; Cui, Y. *Nano Lett.* **2008**, *9* (1), 491−495.
(3) Manthiram, A. *J. Phys. Chem. Lett.* **2011**, *2* (3), 176−184.
(4) Bruce, P. G.; Scrosati, B.; Tarascon, J. M. *Angew. Chem., Int. Ed.* **2008**, *47* (16), 2930−2946.
(5) Li, H.; Liu, X.; Zhai, T.; Li, D.; Zhou, H. *Adv. Energy Mater.* **2012**, *3* (4), 428−432.
(6) Armstrong, A. R.; Lyness, C.; Panchmatia, P. M.; Islam, M. S.; Bruce, P. G. *Nat. Mater.* **2011**, *10* (3), 223−229.
(7) Malini, R.; Uma, U.; Sheela, T.; Ganesan, M.; Renganathan, N. *Ionics* **2009**, *15* (3), 301−307.
(8) (a) Wang, G. J.; Gao, J.; Fu, L. J.; Zhao, N. H.; Wu, Y. P.; Takamura, T. *J. Power Sources* **2007**, *174*, 1109−1112. (b) Kim, H.-K.; Bak, S.-M.; Kim, K.-B. *Electrochem. Commun.* **2010**, *12* (12), 1768−1771.
(9) Ohzuku, T.; Ueda, A.; Yamamoto, N. *J. Electrochem. Soc.* **1995**, *142* (5), 1431−1435.
(10) Chen, J.; Yang, L.; Fang, S.; Hirano, S.-i.; Tachibana, K. *J. Power Sources* **2012**, *200*, 59−66.
(11) Song, J. H.; Park, H. J.; Kim, K. J.; Jo, Y. N.; Kim, J.-S.; Jeong, Y. U.; Kim, Y. J. *J. Power Sources* **2010**, *195* (18), 6157−6161.
(12) Kim, W.-T.; Jeong, Y. U.; Choi, H. C.; Kim, Y. J.; Song, J. H.; Lee, H.; Lee, Y. J. *J. Appl. Electrochem.* **2011**, *41* (7), 803−808.
(13) Kim, W.-T.; Jeong, Y. U.; Lee, Y. J.; Kim, Y. J.; Song, J. H. *J. Power Sources* **2013**, 10.1016/j.jpowsour.2013.01.163.
(14) Lu, C.; Qi, L.; Yang, J.; Wang, X.; Zhang, D.; Xie, J.; Ma, J. *Adv. Mater.* **2005**, *17* (21), 2562−2567.
(15) Lou, X. W.; Wang, Y.; Yuan, C.; Lee, J. Y.; Archer, L. A. *Adv. Mater.* **2006**, *18* (17), 2325−2329.
(16) Yang, J.; Qi, L.; Lu, C.; Ma, J.; Cheng, H. *Angew. Chem., Int. Ed.* **2005**, *44* (4), 598−603.
(17) Laura, J.; Franklin, K.; Huang, J. *J. Am. Chem. Soc.* **2009**, *131*, 1043.
(18) Xiong, Y.; Wiley, B.; Chen, J.; Li, Z. Y.; Yin, Y.; Xia, Y. *Angew. Chem., Int. Ed.* **2005**, *44* (48), 7913−7917.
(19) Wu, Z.-S.; Ren, W.; Wen, L.; Gao, L.; Zhao, J.; Chen, Z.; Zhou, G.; Li, F.; Cheng, H.-M. *ACS Nano* **2010**, *4* (6), 3187−3194.
(20) Wu, X. L.; Jiang, L. Y.; Cao, F. F.; Guo, Y. G.; Wan, L. J. *Adv. Mater.* **2009**, *21* (25−26), 2710−2714.
(21) (a) Tang, W.; Wang, X. J.; Hou, Y. Y.; Li, L. L.; Sun, H.; Zhu, Y. S.; Bai, Y.; Wu, Y. P.; Zhu, K.; van Ree, T. *J. Power Sources* **2012**, *198* (2), 308−311. and (b) Wang, L.; Wang, H.; Liu, Z.; Xiao, C.; Dong, S.; Han, P.; Zhang, Z.; Zhang, X.; Bi, C.; Cui, G. *Solid State Ionics* **2010**, *181* (37), 1685−1689.
(22) Murugan, A. V.; Muraliganth, T.; Manthiram, A. *J. Electrochem. Soc.* **2009**, *156* (2), A79−A83.
(23) Chou, S. L.; Wang, J.; Liu, H.; Dou, S. X. *J. Phys. Chem. C* **2011**, *115* (32), 16220−16227.
(24) Wu, Y. P.; Wan, C. R.; Jiang, C. Y.; Fang, S. B.; Jiang, Y. Y. *Carbon* **1999**, *37* (12), 1901−1908.
(25) (a) Tang, W.; Hou, Y. Y.; Wang, F. X.; Liu, L. L.; Wu, Y. P.; Zhu, K. *Nano Lett.* **2013**, *13* (5), 2036−2040. (b) Qu, Q. T.; Fu, L. J.; Zhan, X. Y.; Samuelis, D.; Li, L.; Guo, W. L.; Li, Z. H.; Wu, Y. P.; Maier, J. *Energy Environ. Sci.* **2011**, *4* (10), 3985−3990.

(26) (a) Lou, X. W.; Li, C. M.; Archer, L. A. *Adv. Mater.* **2009**, *21* (24), 2536−2539. (b) Lou, X. W. D.; Archer, L. A.; Yang, Z. *Adv. Mater.* **2008**, *20* (21), 3987−4019.
(27) Geim, A. K.; Novoselov, K. S. *Nat. Mater.* **2007**, *6* (3), 183−191.
(28) Wang, J.-Z.; Lu, L.; Choucair, M.; Stride, J. A.; Xu, X.; Liu, H.-K. *J. Power Sources* **2011**, *196* (16), 7030−7034.
(29) Persson, K.; Sethuraman, V. A.; Hardwick, L. J.; Hinuma, Y.; Meng, Y. S.; van der Ven, A.; Srinivasan, V.; Kostecki, R.; Ceder, G. *J. Phys. Chem. Lett.* **2010**, *1* (8), 1176−1180.
(30) Uthaisar, C.; Barone, V. *Nano Lett.* **2010**, *10* (8), 2838−2842.
(31) Wu, Z.-S.; Ren, W.; Xu, L.; Li, F.; Cheng, H.-M. *ACS Nano* **2011**, *5* (7), 5463−5471.
(32) Wang, H.; Yang, Y.; Liang, Y.; Robinson, J. T.; Li, Y.; Jackson, A.; Cui, Y.; Dai, H. *Nano Lett.* **2011**, *11* (7), 2644−2647.
(33) Wang, D.; Choi, D.; Li, J.; Yang, Z.; Nie, Z.; Kou, R.; Hu, D.; Wang, C.; Saraf, L. V.; Zhang, J. *ACS Nano* **2009**, *3* (4), 907−914.
(34) Sun, Y.; Wu, Q.; Shi, G. *Energy Environ. Sci.* **2011**, *4* (4), 1113−1132.
(35) Shi, Y.; Chou, S.-L.; Wang, J.-Z.; Wexler, D.; Li, H.-J.; Liu, H.-K.; Wu, Y. *J. Mater. Chem.* **2012**, *22* (32), 16465−16470.